

# Geochemistry of Fluvial Sediments from Geregu, Southwest Nigeria

## Geokemija rečnih sedimentov iz Geregija v SW Nigeriji

**Emmanuel E. Adiotomre\*, Innocent O. Ejeh, Edwin O. Adaikpoh**

Delta State University, Department of Geology, P.M.B. 1, Abraka, Delta State, Nigeria

\*eadiotomre@delsu.edu.ng

### Abstract

Geochemical analysis of fluvial sediments on the banks of River Ero using inductively coupled plasma mass spectrometry illustrates their maturity, provenance and tectonic setting. The analysed sediment samples show low  $\text{SiO}_2/\text{Al}_2\text{O}_3$  ratios of 2.92–2.99 (units FL\_A, FL\_B and FL\_E) and high  $\text{SiO}_2/\text{Al}_2\text{O}_3$  ratios of 4.064–4.852 (units FL\_C, FL\_D, FL\_F and FL\_G). Sediments were geochemically classified as shales (units FL\_A, FL\_B and FL\_E) and greywackes (units FL\_C, FL\_D, FL\_F and FL\_G). Variability in sediment maturity ( $\text{FL}_F > \text{FL}_G > \text{FL}_C > \text{FL}_D > \text{FL}_A > \text{FL}_B > \text{FL}_E$ ) parallels a decreasing order in the ratios of  $\text{SiO}_2/\text{Al}_2\text{O}_3$  and  $\text{K}_2\text{O}/\text{Al}_2\text{O}_3$ , as well as the proportion of quartz grains and matrix components. Evidence from  $\text{Al}_2\text{O}_3/\text{TiO}_2$ ,  $\text{K}_2\text{O}$ , Rb, La/Co, Th/Co, Cr/Th, Th/Cr, La/Th-Hf, Th-Hf-Co and rare earth element contents of sediment samples suggest felsic protoliths of upper continental crust in a passive margin tectonic setting. An insignificant contribution of mafic components from the source is, however, inferred based on the Ni and Cr contents of the sediment samples. Combined Eu anomalies  $<0.85$  and  $(\text{Gd}/\text{Yb})_n$  ratios  $<2.0$  (1.53–1.82, average 1.65) suggest post-Archean protoliths.

**Key words:** Fluvial sediments, Eu anomaly, Southwest Nigeria, Provenance, Tectonic setting

### Povzetek

Geokemijska analiza rečnih sedimentov z bregov reke Ero, opravljena z določitvami induktivno vezane plazemske - masne spektrometrije, priča o njihovi zrelosti, izvoru in geotektonski pripadnosti ozemlja. Analizirani vzorci sedimentov razkrivajo nizke vrednosti razmerja  $\text{SiO}_2/\text{Al}_2\text{O}_3$ , od 2.92 do 2.99, v enotah FL\_A, FL\_B in FL\_E, in visoke vrednosti tega razmerja, od 4.064 do 4.852, v enotah FL\_C, FL\_D, FL\_F in FL\_G. Usedline so geokemično opredelili kot meljevce (enote FL\_A, FL\_B in FL\_E) in drobe (enote FL\_C, FL\_D, FL\_F in FL\_G). Zaporedje usedlin po zrelosti ( $\text{FL}_F > \text{FL}_G > \text{FL}_C > \text{FL}_D > \text{FL}_A > \text{FL}_B > \text{FL}_E$ ) ustreza zaporedju zmanjševanja razmerij  $\text{SiO}_2/\text{Al}_2\text{O}_3$  in  $\text{K}_2\text{O}/\text{Al}_2\text{O}_3$ , deleža kremenovih zrn in sestave osnove. Vrednosti  $\text{Al}_2\text{O}_3/\text{TiO}_2$ ,  $\text{K}_2\text{O}$ , Rb, La/Co, Th/Co, Cr/Th, Th/Cr, La/TH-HF, Th-HF-Co in prvin redkih zemelj, ugotovljene v vzorcih sedimentov, nakazujejo felsične protolite iz vrhnje celinske skorje, umeščene na pasivnem ploščnem robu. Spričo vsebnosti Ni in Cr v sedimentih je možno domnevati majhen prispevek mafičnih komponent. Povezava Eu anomalij  $<0.85$  in razmerja  $(\text{Gd}/\text{Yb})_n$  (1.53–1.82, povprečno 1.65)  $<2.0$  nakazuje protolite poarhajske starosti.

**Ključne besede:** rečni sedimenti, Eu anomalija, SW Nigerija, izvor, tektonska uvrstitev

## Introduction

The geochemistry of clastic sedimentary rocks in terms of major elements, trace elements and rare earth elements (REEs) is widely used to decipher the provenance, tectonic setting and weathering conditions of the source area (e.g. studies by various authors [1–15]). Furthermore, some trace elements (e.g. Y, Sc, Th, Zr, Hf, Cr and Co) and REEs are relatively unaltered in composition during mobilisation from source to sink. This is because of their comparative insolubility in water [16]. Thus, these elements are adequately incorporated in clastic sediments, providing the basis for geochemical characterisation of precursor rocks [2, 4, 6].

The study area is delimited by latitudes 7°33'N and 7°35'N and longitudes 6°40'E and 6°42'E and it is underlain by the Precambrian rocks of the southwestern Nigerian basement complex (Figure 1) [17]. A previous study of clastic sediments on the banks of River Ero in Geregu–Ajaokuta described their textural characteristics and depositional environments [18]. The results define seven stratigraphic units that are dominantly composed of river sand and range in size fraction from fine- to medium-grained sand (Figure 2). The vertical thickness of individual sedimentary layers and their textural characteristics are variable despite the common fluvial depositional environment. Despite existing sedimentological analysis of sedimentary succession on the banks of River Ero in Geregu–Ajaokuta area, including detailed profiles and granulometric data, geochemical data has not been provided so far. The aim of the current study was to investigate the sediment maturity, provenance and tectonic setting of the fluvial sedimentary units on the banks of River Ero, using major elements, trace elements and REEs. Furthermore, because River Ero is a major river that drains the study area and delivers sediments into the River Niger, the information obtained from this study will serve as a proxy to understand the chemical character of the sediments in the deeper Niger River.

## Geological background

The Nigerian basement complex is a component of the Pan-African mobile belt that is located to the east and southwest of the West African and Congo cratons, respectively [19]. The Nigerian basement complex is modified dominantly by the Pan-African thermotectonic event (450–750 Ma) but it also shows a few imprints of older orogenesis, including the Liberan (2500–2750 Ma), Eburnean (2000–2500 Ma) and Kibaran (1100–2000 Ma) [20]. The main rocks that characterise the Nigerian basement complex include the migmatite–gneiss complex, the schist belts and the Pan-African granites [21]. The lithologies included in the migmatite–gneiss complex are gneisses, amphibolites, migmatite and metavolcanics, quartzite and calcareous rocks. The schist belts consist of quartz–mica schist, feldspar–mica schist, talc schists and ferruginous quartzites. The Pan-African granites include rocks such as porphyritic biotite granite and granite gneisses that are medium to coarse grained. The local geology of the Geregu–Ajaokuta area includes major rocks such as porphyritic granite, granite gneiss, migmatite, mica schist and quartzite (Figure 1).

## Materials and methods

Fourteen samples of fluvial sediments for this study were obtained from the exposed sections of six stratigraphic units on the banks of River Ero in Geregu–Ajaokuta, approximately 100 m away from the river mouth. From the fourteen samples collected, seven samples (10 g each) representing each bed were air-dried for 3 days, homogenised (coned and quartered) and analysed to determine their major, trace and REE contents using UT-7 sodium peroxide fusion inductively coupled plasma-mass spectrometry (ICP-MS) at Activation Laboratories Limited, Ancaster, ON, Canada. Geochemical diagrams that included Harker's and Herron's geochemical classifications, elements' bivariate (e.g.  $\text{TiO}_2\text{-Fe}_2\text{O}_3\text{+MgO}$ ,  $\text{Al}_2\text{O}_3\text{/SiO}_2\text{-Fe}_2\text{O}_3\text{+MgO}$  and  $\text{La/Th-Hf}$ ) and ternary plots (e.g.  $\text{V-Ni-Th*10}$  and  $\text{Th-Hf-Co}$ ) as well as chondrite-normalised REE plots were later developed. These plots, coupled with the element ratios [e.g.  $\text{SiO}_2\text{/Al}_2\text{O}_3$ ,

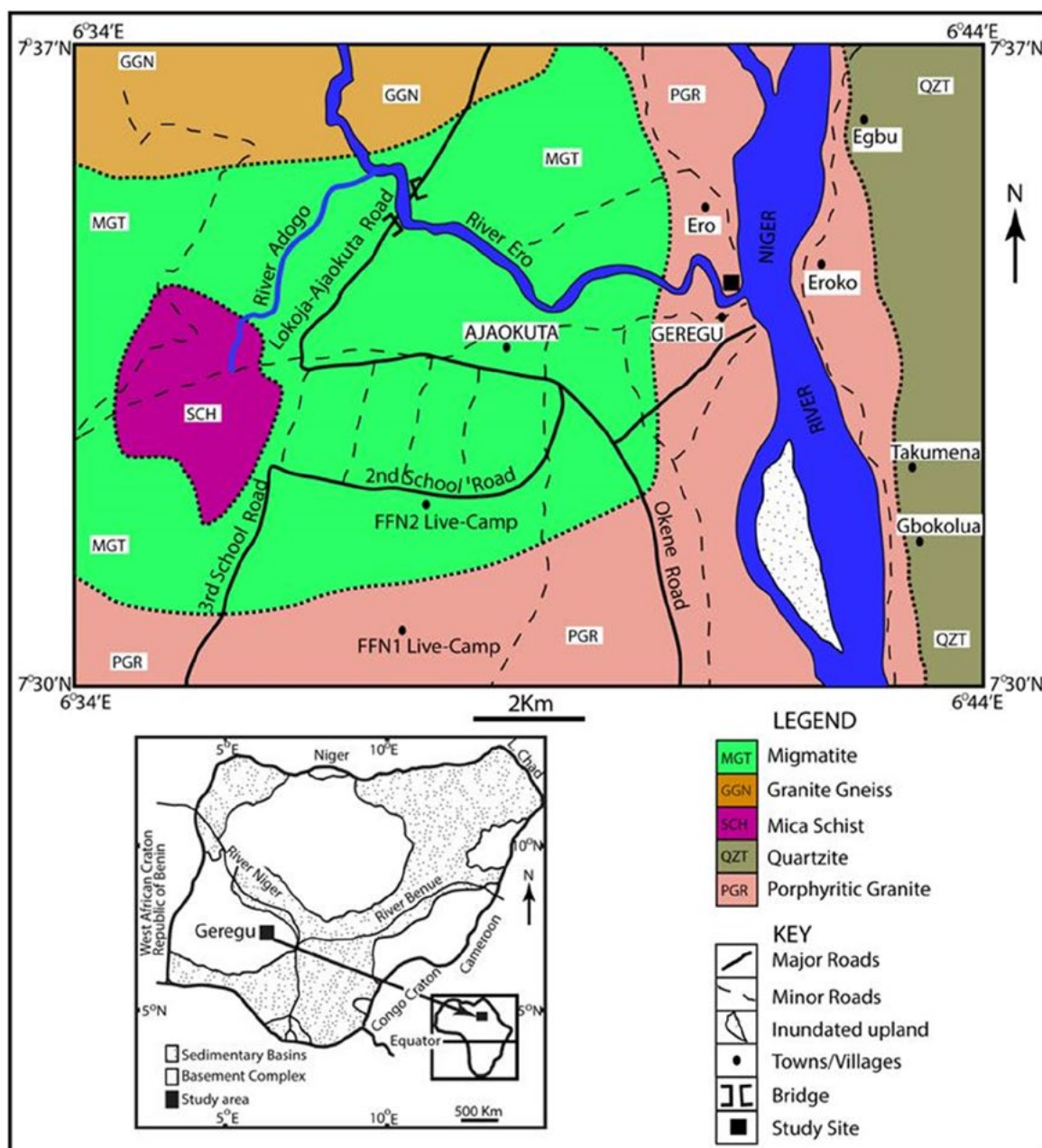


**Figure 1:** Schematic geologic map of the Geregu–Ajaokuta area showing the location of the study site. Inset: Geological map of Nigeria (after Kogbe [17]).

$K_2O/Al_2O_3$ ,  $Al_2O_3/TiO_2$ ,  $Cr/Ni$ ,  $La/Co$ ,  $Th/Co$ ,  $Cr/Th$ ,  $Eu/Eu^*$  and  $(Gd/Yb)_n$ , illustrate the maturity, provenance, tectonic settings and source rock composition of the sediments. Modal estimation of the mineral composition of the sediment samples was conducted combining the Gazzi–Dickinson method [22–23] and standard methods with 200 mineral grains counted in every thin section.

## Results

### *Textural and mineralogical composition*

A previous study has shown that the Geregugu clastic sediments have a mean grain size that varies between 3.29  $\phi$  and 1.31  $\phi$ , with standard deviation values (s) ranging from 0.62  $\phi$  to 2.27  $\phi$  (Table 1) [18]. These results suggest that the sediments are medium-to-very fine sands and are moderately to very poorly sorted.

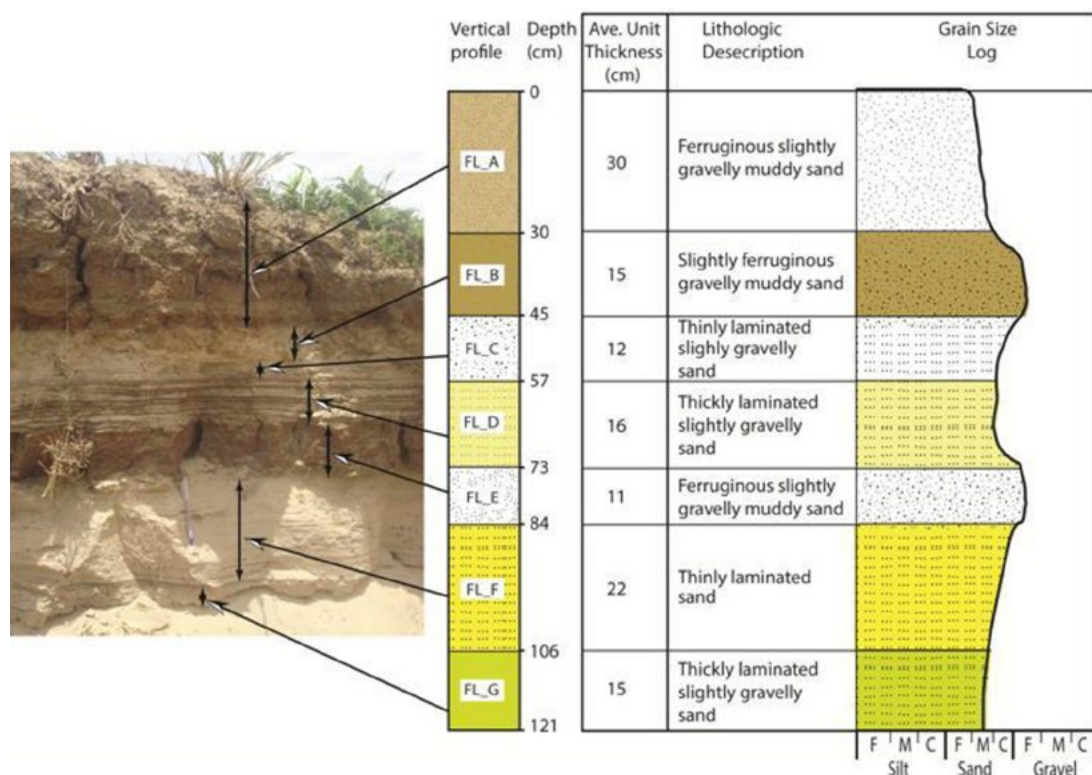


**Figure 2:** Lithostratigraphic column showing the sequence of fluvial sediments and their sedimentological characteristics (after Adiotomre et al. [18]).

**Table 1:** Granulometric data and average modal composition (in %) of the Geregu fluvial sediments

| Sample code     | FL_A | FL_B | FL_C | FL_D | FL_E | FL_F | FL_G |
|-----------------|------|------|------|------|------|------|------|
| Mz <sup>a</sup> | 2.85 | 1.31 | 3.29 | 3.15 | 2.53 | 3.01 | 3.10 |
| σ <sup>a</sup>  | 2.17 | 2.16 | 0.74 | 0.67 | 2.27 | 0.63 | 0.62 |
| Qt              | 42   | 46   | 54   | 49   | 38   | 58   | 54   |
| Ft              | 2    | 3    | 1    | 4    | 2    | 4    | 4    |
| Lf              | 1    | 2    | 1    | 2    | 1    | 1    | 2    |
| Mica            | 1    | 1    | 2    | 1    | 2    | 1    | 2    |
| Opaque          | 11   | 10   | 5    | 6    | 10   | 5    | 6    |
| Matrix          | 43   | 38   | 37   | 38   | 47   | 31   | 32   |

Note: <sup>a</sup>Adiotomre et al. [18]; Mz: particle size (φ); σ: sorting (φ); Qt: total quartz (monocrystalline and polycrystalline quartz); Ft: total feldspar; Lf: lithic fragments.

The average modal estimation of the mineralogical composition of the studied sediment samples reveals that quartz is the dominant component (38–58%), followed by matrix (31–47%), opaque (5–11%), feldspar (1–4%), mica (1–2%) and lithic fragments (1–2%) (Table 1). The average quartz–feldspar–lithic

fragment (QtFtLf) ratios are Qt<sub>42</sub>Ft<sub>2</sub>Lf<sub>1</sub> (FL\_A), Qt<sub>46</sub>Ft<sub>3</sub>Lf<sub>2</sub> (FL\_B), Qt<sub>54</sub>Ft<sub>1</sub>Lf<sub>1</sub> (FL\_C), Qt<sub>49</sub>Ft<sub>4</sub>Lf<sub>2</sub> (FL\_D), Qt<sub>38</sub>Ft<sub>2</sub>Lf<sub>1</sub> (FL\_E), Qt<sub>58</sub>Ft<sub>4</sub>Lf<sub>1</sub> (FL\_F) and Qt<sub>54</sub>Ft<sub>4</sub>Lf<sub>2</sub> (FL\_G). The matrix between the sand grains contains some unresolved (petrographically) mineral grains that are probably clays.

**Table 2:** Major element average contents (in weight percent oxide) in the Geregu fluvial sediments and PAAS.

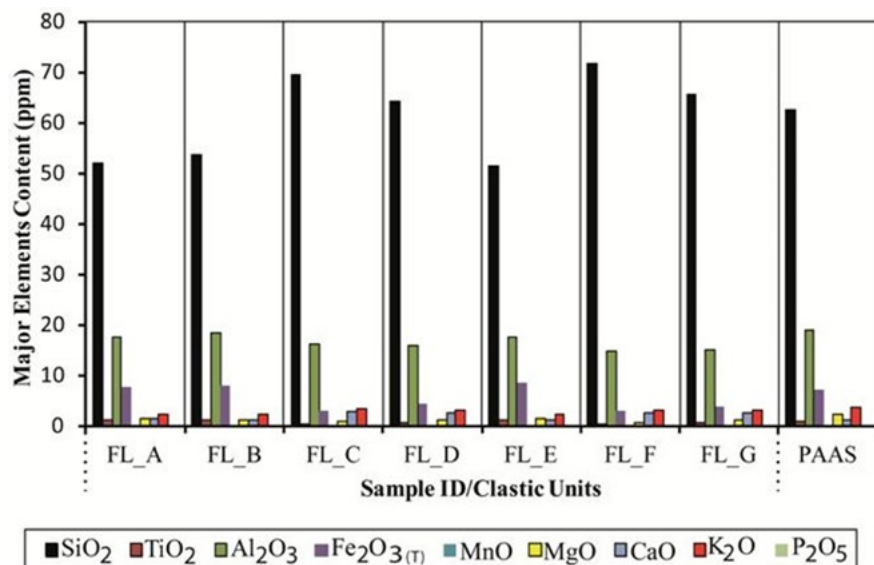
| Sample code   | FL_A                                     | FL_B                                     | FL_C                                    | FL_D                                     | FL_E                                     | FL_F                  | FL_G                                     | PAAS  |
|---|--|--|---|--|--|-----------------------|--|-------|
| <b>Textural description<sup>a</sup></b>                 | Ferruginous slightly gravelly muddy sand | Slightly ferruginous gravelly muddy sand | Thinly laminated slightly gravelly sand | Thickly laminated slightly gravelly sand | Ferruginous slightly gravelly muddy sand | Thinly laminated sand | Thickly laminated slightly gravelly sand | -     |
| <b>Depth (cm)<sup>a</sup></b>                           | 030                                      | 045                                      | 057                                     | 073                                      | 084                                      | 106                   | 121                                      |       |
| <b>Thickness (cm)<sup>a</sup></b>                       | 30                                       | 15                                       | 12                                      | 16                                       | 11                                       | 22                    | 15                                       |       |
| <b>SiO<sub>2</sub> [0.01]</b>                           | 52.02                                    | 53.70                                    | 69.52                                   | 64.13                                    | 51.45                                    | 71.61                 | 65.50                                    | 62.40 |
| <b>TiO<sub>2</sub> [0.01]</b>                           | 1.02                                     | 1.03                                     | 0.46                                    | 0.53                                     | 1.07                                     | 0.38                  | 0.48                                     | 0.99  |
| <b>Al<sub>2</sub>O<sub>3</sub> [0.01]</b>               | 17.43                                    | 18.36                                    | 16.17                                   | 15.78                                    | 17.64                                    | 14.76                 | 14.94                                    | 18.80 |
| <b>Fe<sub>2</sub>O<sub>3</sub><sup>(T)</sup> [0.05]</b> | 7.58                                     | 7.97                                     | 2.91                                    | 4.35                                     | 8.62                                     | 2.85                  | 3.79                                     | 7.18  |
| <b>MnO [0.0004]</b>                                     | 0.15                                     | 0.13                                     | 0.05                                    | 0.06                                     | 0.13                                     | 0.04                  | 0.05                                     | 0.11  |
| <b>MgO [0.01]</b>                                       | 1.32                                     | 1.24                                     | 0.82                                    | 1.20                                     | 1.36                                     | 0.62                  | 1.11                                     | 2.19  |
| <b>Na<sub>2</sub>O</b>                                  | -  | -  | -                                       | -  | -  | -                     | -  | 1.19  |
| <b>CaO [0.01]</b>                                       | 1.50                                     | 1.13                                     | 2.74                                    | 2.52                                     | 1.26                                     | 2.59                  | 2.48                                     | 1.29  |
| <b>K<sub>2</sub>O [0.1]</b>                             | 2.27                                     | 2.33                                     | 3.37                                    | 3.18                                     | 2.26                                     | 3.18                  | 3.05                                     | 3.68  |
| <b>P<sub>2</sub>O<sub>5</sub> [0.005]</b>               | 0.14                                     | 0.11                                     | 0.05                                    | 0.07                                     | 0.14                                     | 0.04                  | 0.05                                     | 0.16  |
| <b>Fe<sub>2</sub>O<sub>3(T)</sub>+MgO</b>               | 8.9                                      | 9.21                                     | 3.73                                    | 5.55                                     | 9.98                                     | 3.47                  | 4.9                                      | -     |
| <b>Al<sub>2</sub>O<sub>3</sub>/TiO<sub>2</sub></b>      | 17.088                                   | 17.825                                   | 35.152                                  | 29.774                                   | 16.486                                   | 38.842                | 31.125                                   | -     |
| <b>Al<sub>2</sub>O<sub>3</sub>/SiO<sub>2</sub></b>      | 0.335                                    | 0.342                                    | 0.233                                   | 0.246                                    | 0.343                                    | 0.206                 | 0.228                                    | -     |
| <b>SiO<sub>2</sub>/Al<sub>2</sub>O<sub>3</sub></b>      | 2.985                                    | 2.925                                    | 4.299                                   | 4.064                                    | 2.917                                    | 4.852                 | 4.384                                    | -     |
| <b>K<sub>2</sub>O/Al<sub>2</sub>O<sub>3</sub></b>       | 0.130                                    | 0.127                                    | 0.208                                   | 0.202                                    | 0.128                                    | 0.215                 | 0.204                                    | -     |
| <b>Fe<sub>2</sub>O<sub>3(T)</sub>/K<sub>2</sub>O</b>    | 3.339                                    | 3.421                                    | 0.864                                   | 1.368                                    | 3.814                                    | 0.896                 | 1.243                                    | -     |

Note: <sup>a</sup>Adiotomre *et al.* [18]; PAAS: post-Archean Australian shale [16]; Fe<sub>2</sub>O<sub>3(T)</sub> = total Fe. Values in square brackets are the detection limits for individual oxides.

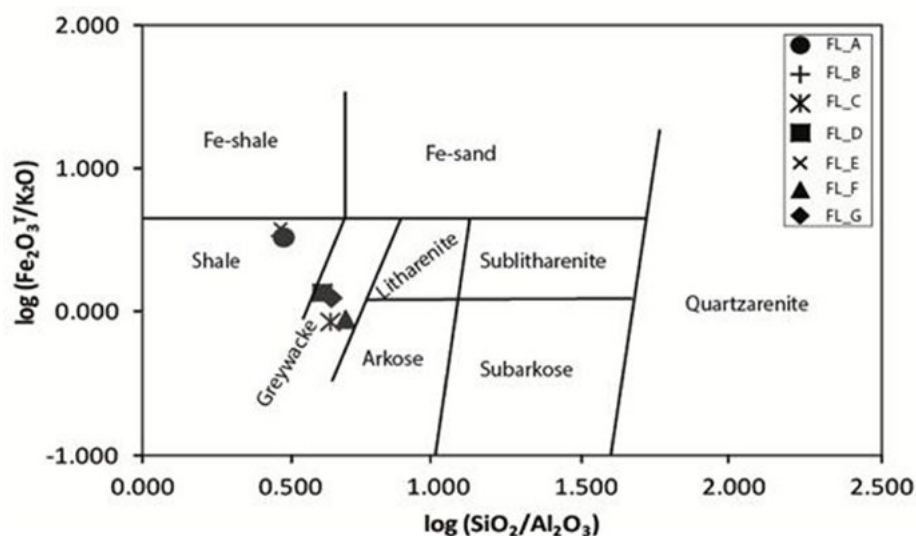
### Major element geochemistry

Table 2 presents the results of the major element analysis of the Geregu fluvial sediments. The major element composition of the post-Archean Australian shale (PAAS), as proposed by Taylor and McLennan [16], is also listed for comparison. Table 2 and Figure 3 illustrate that the clastic stratigraphic units (FL\_A, FL\_B, FL\_C, FL\_D, FL\_E and FL\_F) range from 51.45 to 71.61 weight percent in terms of the SiO<sub>2</sub> content, with the greatest value associated with Unit FL\_F, which is dominantly sand, and the least content occurs in Unit FL\_E, which is slightly gravelly muddy sand. Generally, the SiO<sub>2</sub> content of the fluvial sediments is higher in the sand-sized fractions (FL\_C, FL\_D, FL\_F and FL\_G) than in the silt and clay-sized fractions (FL\_A, FL\_B and FL\_E). The plot of Herron [24], shown in Figure 4, depicts this observation.

Stratigraphic units FL\_A, FL\_B and FL\_E are depleted in SiO<sub>2</sub> content and enriched in the weight percent of oxides of most of the major elements listed in Table 2. These units are, however, depleted in CaO and K<sub>2</sub>O. Conversely, stratigraphic units FL\_C, FL\_D, FL\_F and FL\_G are relatively enhanced in SiO<sub>2</sub>, CaO and K<sub>2</sub>O and depleted in TiO<sub>2</sub>, Al<sub>2</sub>O<sub>3</sub>, Fe<sub>2</sub>O<sub>3(T)</sub>, MnO, MgO and P<sub>2</sub>O<sub>5</sub> (Table 2). Evidently, the positive correlation between SiO<sub>2</sub> and the oxides of Ca and K, as well as the negative correlation that exists between SiO<sub>2</sub> and elements such as TiO<sub>2</sub>, Al<sub>2</sub>O<sub>3</sub>, Fe<sub>2</sub>O<sub>3(T)</sub>, MnO, MgO and P<sub>2</sub>O<sub>5</sub>, clearly demonstrates this relationship (Table 2; Figure 5). Unit FL\_E, however, has a lower K<sub>2</sub>O (2.26 weight%) as compared to other units of the stratigraphic sequence and a CaO content (1.26 weight%) that is only slightly higher than the CaO content of Unit FL\_B (1.13 weight%; Table 2). In addition,



**Figure 3:** Histogram showing the concentrations of the oxides of the major elements in the Geregu fluvial sediments. PAAS = post-Archean Australian shale (after Taylor and McLennan [16]).



**Figure 4:** Plot of  $\log (\text{Fe}_2\text{O}_3/\text{K}_2\text{O})$  versus  $\log (\text{SiO}_2/\text{Al}_2\text{O}_3)$  showing the chemical fields of the Geregu fluvial sediments (FL\_A – FL\_G) (fields after Herron [24]).

Unit FL\_E is lower in  $\text{Al}_2\text{O}_3$  (17.64 weight%) than Unit FL\_B (18.36 weight%). Units FL\_A, FL\_B and FL\_E have depleted  $\text{SiO}_2$  content, while units FL\_C, FL\_D, FL\_F and FL\_G are enriched in  $\text{SiO}_2$  as compared to the PAAS (Table 2).  $\text{Al}_2\text{O}_3$ , MgO,  $\text{K}_2\text{O}$  and  $\text{P}_2\text{O}_5$  contents in units FL\_A, FL\_B and FL\_E are low as compared to those of the PAAS but are comparatively enriched in units FL\_C, FL\_D, FL\_F and FL\_G (Table 2). It is also seen from Table 2 that when compared with

PAAS, units FL\_C, FL\_D, FL\_F and FL\_G are depleted in  $\text{TiO}_2$ ,  $\text{Fe}_2\text{O}_3$  and MnO. However, units FL\_A, FL\_B and FL\_E are enriched in these oxides. A somewhat different trend in CaO distribution however occurs. Units FL\_A, FL\_C, FL\_D, FL\_F and FL\_G are enriched in CaO, while units FL\_B and FL\_E are depleted in CaO relative to PAAS.

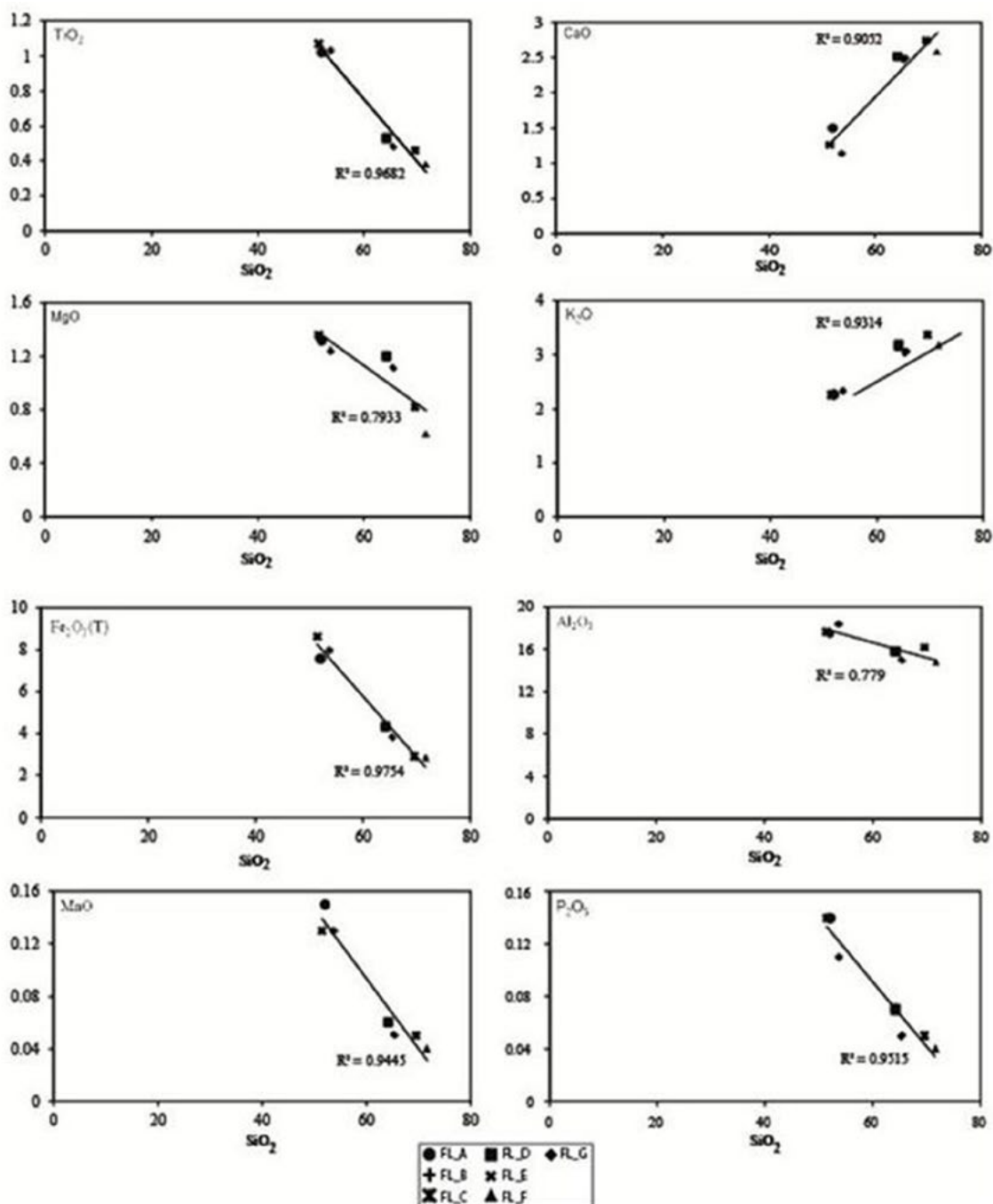


Figure 5: Harker's variation plots for the Geregu fluvial sediments.

### Trace element geochemistry

Table 3 and Figure 6 illustrate the trace element composition of the analysed clastic stratigraphic units. Units FL\_A, FL\_B and FL\_E, which are relatively low in  $\text{SiO}_2$  (51.45–53.70 weight%), have high content of most of the analysed trace elements (1.6–310 ppm), as compared to units

FL\_C, FL\_D, FL\_F and FL\_G, which have high proportion of  $\text{SiO}_2$  (64.13–71.61 weight%) and are depleted in the same trace elements (<0.2–100 ppm). However, variation occurs with Ba and Sr. The Ba and Sr contents are low (707–800 ppm and 163–200 ppm, respectively) in stratigraphic units (FL\_A, FL\_B and FL\_E)

**Table 3:** Average trace element contents (in ppm) in the Geregü fluvial sediments and in PAAS.

| Sample code                             | FL_A                                     | FL_B                                     | FL_C                                    | FL_D                                    | FL_E                                     | FL_F                  | FL_G                                     | PAAS |
|---|--|--|---|---|--|-----------------------|--|------|
| <b>Textural description<sup>a</sup></b> | Ferruginous slightly gravelly muddy sand | Slightly ferruginous gravelly muddy sand | Thinly laminated slightly gravelly sand | Thickly laminated lightly gravelly sand | Ferruginous slightly gravelly muddy sand | Thinly laminated sand | Thickly laminated slightly gravelly sand |      |
| <b>Depth (cm)<sup>a</sup></b>           | 30                                       | 45                                       | 57                                      | 73                                      | 84                                       | 106                   | 121                                      |      |
| <b>Thickness (cm)<sup>a</sup></b>       | 30                                       | 15                                       | 12                                      | 16                                      | 11                                       | 22                    | 15                                       |      |
| <b>Cs [0.1]</b>                         | 3.2                                      | 3.6                                      | 1.1                                     | 1.9                                     | 3.7                                      | 0.70                  | 1.7                                      | -    |
| <b>Ni [10]</b>                          | 70                                       | 130                                      | 60                                      | 40                                      | 70                                       | 10                    | 40                                       | 55   |
| <b>Ga [0.2]</b>                         | 24.8                                     | 27                                       | 18.2                                    | 19.7                                    | 25                                       | 16.5                  | 19                                       | -    |
| <b>Nb [2.4]</b>                         | 23.9                                     | 21.4                                     | 7.6                                     | 8.7                                     | 21                                       | 7.4                   | 7.7                                      | 1.9  |
| <b>Ba [3.0]</b>                         | 800                                      | 777                                      | 1190                                    | 1110                                    | 707                                      | 1220                  | 1070                                     | 650  |
| <b>Ta [0.2]</b>                         | 0.16                                     | 1.6                                      | 0.60                                    | 0.60                                    | 1.6                                      | 0.80                  | 0.60                                     | -    |
| <b>Co [0.2]</b>                         | 23.5                                     | 70                                       | <0.2                                    | 14.4                                    | 23.5                                     | <0.2                  | <0.2                                     | 23   |
| <b>Cu [2.0]</b>                         | 50                                       | 53                                       | 28                                      | 28                                      | 51                                       | 18                    | 21                                       | 50   |
| <b>Sr [3.0]</b>                         | 200                                      | 183                                      | 442                                     | 409                                     | 163                                      | 429                   | 385                                      | 200  |
| <b>V [5.0]</b>                          | 105                                      | 128                                      | 50                                      | 67                                      | 102                                      | 39                    | 55                                       | 96   |
| <b>Zn [30.0]</b>                        | 100                                      | 110                                      | 30                                      | 80                                      | 110                                      | <30                   | 50                                       | 85   |
| <b>Th [0.1]</b>                         | 25.5                                     | 21.5                                     | 11.5                                    | 12.7                                    | 24.1                                     | 12.5                  | 9.3                                      | 15   |
| <b>U [0.1]</b>                          | 5.7                                      | 4.8                                      | 2.5                                     | 2.4                                     | 6.4                                      | 1.8                   | 2.1                                      | -    |
| <b>Cr [30.0]</b>                        | 120                                      | 310                                      | 30                                      | 60                                      | 160                                      | 70                    | 100                                      | 110  |
| <b>Rb [0.4]</b>                         | 111                                      | 116                                      | 76.4                                    | 93.3                                    | 115                                      | 62.8                  | 86.8                                     | 160  |
| <b>Hf [10.0]</b>                        | 20                                       | <10                                      | 10                                      | <10                                     | <10                                      | <10                   | <10                                      | 5    |
| <b>Y [0.1]</b>                          | 49.3                                     | 43                                       | 15.8                                    | 19.7                                    | 48.2                                     | 12.3                  | 17.1                                     | 27   |
| <b>Cr/Th</b>                            | 4.71                                     | 14.42                                    | 2.61                                    | 4.72                                    | 6.64                                     | 5.60                  | 10.75                                    | 7.33 |
| <b>Th/Cr</b>                            | 0.21                                     | 0.07                                     | 0.38                                    | 0.21                                    | 0.15                                     | 0.18                  | 0.09                                     | 0.14 |
| <b>Th/Co</b>                            | 1.09                                     | 0.31                                     | 59.9                                    | 0.88                                    | 1.03                                     | 64.43                 | 48.19                                    | 0.65 |
| <b>Th/U</b>                             | 4.47                                     | 4.48                                     | 4.6                                     | 5.29                                    | 3.77                                     | 6.94                  | 4.43                                     | -    |
| <b>Rb/Sr</b>                            | 0.56                                     | 0.63                                     | 0.17                                    | 0.23                                    | 0.71                                     | 0.15                  | 0.23                                     | 0.80 |
| <b>Cr/V</b>                             | 1.14                                     | 2.42                                     | 0.6                                     | 0.9                                     | 1.57                                     | 1.79                  | 1.82                                     | 1.15 |
| <b>Y/Ni</b>                             | 0.70                                     | 0.33                                     | 0.26                                    | 0.49                                    | 0.69                                     | 1.23                  | 0.43                                     | 0.49 |
| <b>Cr/Ni</b>                            | 1.71                                     | 2.38                                     | 0.50                                    | 1.50                                    | 2.29                                     | 7.00                  | 2.50                                     | 2.00 |
| <b>Cr/Ba</b>                            | 0.15                                     | 0.40                                     | 0.03                                    | 0.05                                    | 0.23                                     | 0.06                  | 0.09                                     | 0.17 |

Note: <sup>a</sup>Adiotomre *et al.* [18]; PAAS: post-Archean Australian shale [16]. Values in square brackets are the detection limits for individual oxides.

that are relatively low in silica, as compared to units (FL\_C, FL\_D, FL\_F and FL\_G) that have high contents of Ba and Sr (1070–1220 ppm and 385–442 ppm, respectively). Units FL\_C, FL\_D and FL\_F are high in Ba and Sr contents and are low in Rb, as compared to units FL\_A, FL\_B and FL\_E, which have low Ba and Sr contents but are high in Rb. Similarly, units FL\_C, FL\_D and FL\_F have depleted contents of Th and U, as compared to units FL\_A, FL\_B and FL\_E, which have high Th and U contents (Table 3; Figure 6). Overall, stratigraphic units that have depleted contents of Ba and Rb content are comparatively enriched in Th and U. Furthermore, units

FL\_C, FL\_D, FL\_F and FL\_G are depleted in high field strength elements such as Nb and Y, which are relatively enriched in units FL\_A, FL\_B and FL\_E. The high field strength elements (e.g. Nb and Y) are analogous to the transitional trace elements such as Cr, V and Co in the way that they vary in proportion in the studied sediment samples. For instance, Cr, V and Co (transition trace elements) and Nb and Y (high field strength elements) are high in units FL\_A, FL\_B and FL\_E but depleted in units FL\_C, FL\_D, FL\_F and FL\_G. Compared to the trace element contents in PAAS, units FL\_A, FL\_B and FL\_E are higher in Cr, V and Co content, while units FL\_C,



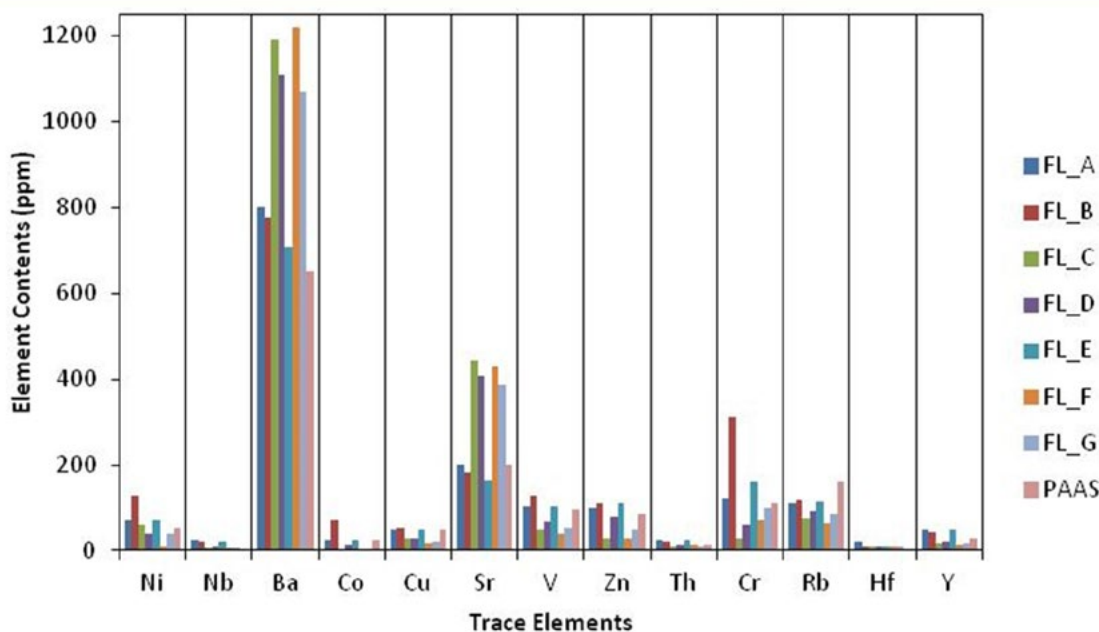


Figure 6: Histogram showing trace element concentrations of the Geregu fluvial sediments.

FL\_D, FL\_F and FL\_G have low contents as compared to PAAS (Table 3; Figure 6). In contrast to Ba and Hf, which are abundant in the studied sediment samples, Rb is low in content as compared to PAAS. Units FL\_C, FL\_D, FL\_F and FL\_G are more enriched in Sr relative to PAAS, while units FL\_A, FL\_B and FL\_E are depleted or have Sr content that is equal to that in PAAS. Conversely, units FL\_A, FL\_B and FL\_E have enriched Cu and Th contents but these elements are depleted in units FL\_C, FL\_D, FL\_F and FL\_G as compared to the levels in PAAS. Nb is higher in content in the studied stratigraphic units than in PAAS, while Y is more enriched in units FL\_A, FL\_B and FL\_E but depleted in units FL\_C, FL\_D, FL\_F and FL\_G relative to the levels in PAAS. The analysed stratigraphic units, however, show a contrary order in Ni and Zn contents with respect to PAAS such that units FL\_A, FL\_B, FL\_C and FL\_E are higher in Ni content, while units FL\_A, FL\_B and FL\_E are more enriched in Zn compared with the levels in PAAS.

A positive correlation exists between  $Al_2O_3$  and transition elements such as Cr, V and Co in the analysed sediment samples; a more positive correlation, however, occurs with V ( $R^2=0.8981$ ) while the least correlation ( $R^2=0.571$ ) exists with Cr (Figure 7).

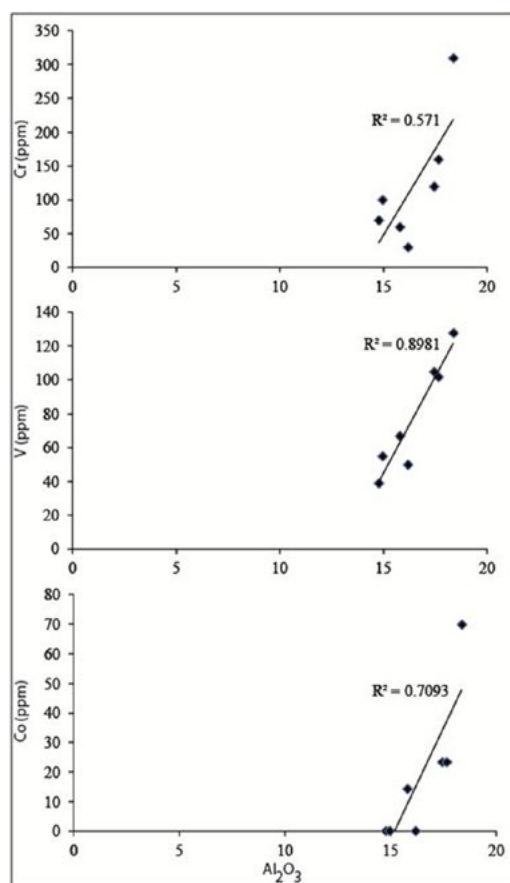


Figure 7: Plots of Cr, V and Co versus  $Al_2O_3$  for the Geregu fluvial sediments.

**Table 4:** Rare earth element average contents (in ppm) in the Geregú fluvial sediments and the PAAS.

| Sample code                             | FL_A                         | FL_B                | FL_C                                    | FL_D                                     | FL_E                         | FL_F                  | FL_G                                     | PAAS   | CI-chondrites |
|---|------------------------------|---------------------|---|--|------------------------------|-----------------------|--|--------|---------------|
| <b>Textural description<sup>a</sup></b> | Slightly gravelly muddy sand | Gravelly muddy sand | Thinly laminated slightly gravelly sand | Thickly laminated slightly gravelly sand | Slightly gravelly muddy sand | Thinly laminated sand | Thickly laminated slightly gravelly sand |        |               |
| <b>Depth (cm)<sup>a</sup></b>           | 30                           | 45                  | 57                                      | 73                                       | 84                           | 106                   | 121                                      |        |               |
| <b>Thickness (cm)<sup>a</sup></b>       | 30                           | 15                  | 12                                      | 16                                       | 11                           | 22                    | 15                                       |        |               |
| <b>La [0.4]</b>                         | 86.1                         | 70.8                | 25.3                                    | 32.6                                     | 81.7                         | 16.5                  | 23.4                                     | 038    | 0.235         |
| <b>Ce [0.8]</b>                         | 188                          | 142                 | 59.4                                    | 75.7                                     | 177                          | 39.9                  | 53.2                                     | 080    | 0.600         |
| <b>Pr [0.1]</b>                         | 020                          | 15.4                | 06.4                                    | 7.8                                      | 18.6                         | 4.3                   | 5.8                                      | 8.83   | 0.091         |
| <b>Nd [0.4]</b>                         | 072                          | 55.4                | 22.5                                    | 28.3                                     | 66.4                         | 15.5                  | 20.7                                     | 33.9   | 0.464         |
| <b>Sm [0.1]</b>                         | 13.3                         | 10.5                | 04.3                                    | 05.4                                     | 11.8                         | 03.2                  | 004                                      | 5.55   | 0.153         |
| <b>ΣLREE</b>                            | 379.4                        | 294.1               | 117.9                                   | 149.8                                    | 355.5                        | 79.4                  | 107.1                                    | 166.28 | 1.543         |
| <b>Eu [0.1]</b>                         | 02.7                         | 02.2                | 01.1                                    | 01.4                                     | 02.6                         | 0.90                  | 01.2                                     | 1.08   | 0.0586        |
| <b>Gd [0.1]</b>                         | 12.2                         | 10                  | 3.9                                     | 4.9                                      | 11.6                         | 3                     | 3.9                                      | 4.66   | 0.206         |
| <b>Tb [0.1]</b>                         | 1.7                          | 1.4                 | 0.6                                     | 0.7                                      | 1.6                          | 0.4                   | 0.6                                      | 0.77   | 0.0375        |
| <b>Dy [0.3]</b>                         | 8.7                          | 7.3                 | 2.7                                     | 3.3                                      | 8.1                          | 2.1                   | 3  | 4.68   | 0.254         |
| <b>Ho [0.2]</b>                         | 1.9                          | 1.6                 | 0.6                                     | 0.7                                      | 1.7                          | 0.5                   | 0.6                                      | 0.99   | 0.0566        |
| <b>Er [0.1]</b>                         | 5.9                          | 4.9                 | 1.9                                     | 2.3                                      | 5.6                          | 1.4                   | 2.0                                      | 2.85   | 0.166         |
| <b>Tm [0.1]</b>                         | 0.8                          | 0.7                 | 0.3                                     | 0.3                                      | 0.7                          | 0.2                   | 0.3                                      | 0.4    | 0.0262        |
| <b>Yb [0.1]</b>                         | 5.7                          | 4.9                 | 2.1                                     | 2.2                                      | 5.5                          | 1.6                   | 2.0                                      | 2.82   | 0.168         |
| <b>ΣHREE</b>                            | 39.6                         | 33                  | 13.2                                    | 15.8                                     | 37.4                         | 10.1                  | 13.6                                     | 18.25  | 0.9729        |
| <b>ΣREE</b>                             | 419                          | 327.1               | 131.1                                   | 165.6                                    | 392.9                        | 89.5                  | 120.7                                    | 184.53 | 2.5159        |
| <b>ΣLREE/ΣHREE</b>                      | 9.58                         | 8.91                | 8.93                                    | 9.48                                     | 9.51                         | 7.86                  | 7.88                                     | 9.11   | 1.59          |
| <b>Eu*</b>                              | 4.24                         | 3.40                | 1.37                                    | 1.72                                     | 3.87                         | 1.03                  | 1.31                                     | -      | -             |
| <b>Σ-Eu</b>                             | 0.64                         | 0.65                | 0.81                                    | 0.82                                     | 0.67                         | 0.87                  | 0.92                                     | 0.66   | -             |
| <b>La/Th</b>                            | 3.38                         | 3.29                | 2.2                                     | 2.57                                     | 3.39                         | 1.32                  | 2.52                                     | 2.53   | -             |
| <b>La/Yb</b>                            | 15.11                        | 14.45               | 12.05                                   | 14.82                                    | 14.85                        | 10.31                 | 11.70                                    | 13.48  |               |
| <b>(La/Yb)<sub>n</sub></b>              | 10.80                        | 10.33               | 8.61                                    | 10.59                                    | 10.62                        | 7.38                  | 8.37                                     | 9.2    |               |
| <b>Ce/La</b>                            | 2.18                         | 2.01                | 2.35                                    | 2.32                                     | 2.17                         | 2.42                  | 2.27                                     | 2.11   |               |
| <b>La/Ni</b>                            | 1.23                         | 0.54                | 0.42                                    | 0.82                                     | 1.17                         | 1.65                  | 0.59                                     | 1.23   |               |
| <b>Gd/Yb</b>                            | 2.14                         | 2.04                | 1.86                                    | 2.23                                     | 2.11                         | 1.88                  | 1.95                                     | 1.65   |               |
| <b>(Gd/Yb)<sub>n</sub></b>              | 1.75                         | 1.66                | 1.51                                    | 1.82                                     | 1.72                         | 1.53                  | 1.59                                     | 1.35   |               |

Note: <sup>a</sup>Adiotomre et al. [18]; PAAS: post-Archean Australian shale [16]; CI-chondrite, after Barat et al. [25];  $\gamma$ -Eu: Eu anomaly;  $\gamma$ -Eu = Eu/Eu\*; Eu\* = (Sm + Gd)/2;  $\gamma$ -Eu computed after Tang et al. [26]. Values in square brackets are the detection limits for individual oxides.

### REE geochemistry

Table 4 illustrates the REE concentration in the Geregú clastic sediments. The light REEs (LREEs) vary from 3.2 to 188 ppm, while the heavy REEs (HREEs) range from 0.2 to 12.2 ppm. In general, there is a systematic variation in the REE contents of the clastic stratigraphic units. Sedimentary units that are relatively depleted in SiO<sub>2</sub> (e.g. units FL\_A, FL\_B and FL\_E) are high in REE contents (Table 4). Conversely, sedimentary units that are comparatively enriched in SiO<sub>2</sub> (e.g. units FL\_C, FL\_D,

FL\_F and FL\_G) have low REE concentrations (Table 4). It is clear from Table 4 that stratigraphic units FL\_A (ferruginous and slightly gravelly muddy sand) and FL\_F (sandy) have the highest and lowest concentrations of REE, respectively. Table 4 also illustrates that the SL-REE and SHREE concentrations in the analysed samples of the sedimentary units systematically increase as the mud (i.e. fine fractions) part of the sediments increases.

Figure 8 and Table 4 show much enrichment in LREE over the HREE in the analysed samples,

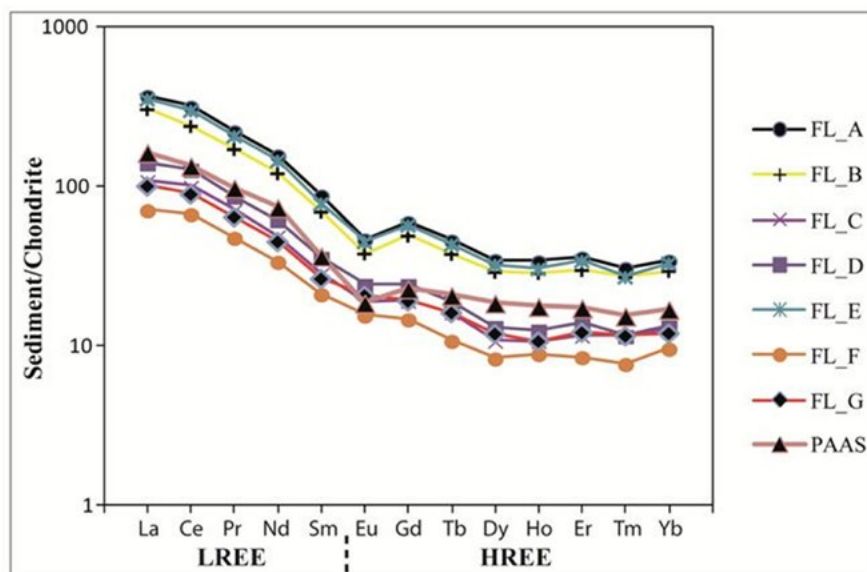


Figure 8: Rare earth element (REE) patterns in the Geregu fluvial sediments and the PAAS, normalised to the average chondrite.

corroborated by the  $(La/Yb)_n$  values of 7.38–10.80. The HREE and LREE patterns illustrated in the chondrite-normalised plots are steep and flat, respectively, and it is probably due to the high fractionation of the LREE over the HREE. The SREE content in the analysed samples of the stratigraphic units FL\_A, FL\_B and FL\_E (327.1–419 ppm) is higher than the SREE concentration (184.53 ppm) in the PAAS (Table 4; Figure 8), whereas the SREE concentration in units FL\_C, FL\_D, FL\_F and FL\_G (89.5–165.6 ppm) is lower than the SREE in PAAS (Table 4; Figure 8). Overall, the REE patterns for the studied stratigraphic units are similar to those in PAAS and show distinct negative Eu anomalies (Figure 8). Units FL\_A, FL\_B and FL\_E have marked negative Eu anomaly ( $Eu/Eu^* = 0.64–0.67$ ), which is the same as in PAAS (0.66). On the other hand, units FL\_C, FL\_D, FL\_F and FL\_G are characterised by insignificant negative Eu anomaly ( $Eu/Eu^* = 0.81–0.92$ ) (Table 4). Units FL\_A, FL\_B, FL\_D and FL\_E have  $(La/Yb)_n$  values that range between 10.33 and 10.80, which are higher than the  $(La/Yb)_n$  values in the units FL\_C, FL\_F and FL\_G (7.38–8.61) and in PAAS (9.2) (Table 4). Furthermore,  $(Gd/Yb)_n$  is higher (1.66–1.75) for units FL\_A, FL\_B, FL\_D and FL\_E than for units FL\_C, FL\_F and FL\_G (1.51–1.59), as well as for PAAS (1.35) (Table 4).

## Discussion

### Sediment maturity

The interpretation of maturity for the fluvial sediments was done with regard to textural characteristics, as well as the mineralogical and chemical compositions (Tables 1 and 2). Based on sorting, the sediments are immature (FL\_C, FL\_D, FL\_F and FL\_G) to more immature (FL\_A, FL\_B and FL\_E). Mineralogically, the sediments are characterised by high matrix content (31–47%), which suggests immaturity. Sediment maturity in the form of chemical transformation of the sedimentary clastics relates to observable ratios of  $SiO_2/Al_2O_3$  and  $K_2O/Al_2O_3$  because these ratios vary as sediment maturity changes (e.g. the work of Le Maitre [27]). The  $SiO_2/Al_2O_3$  ratios for the analysed sedimentary units range from 2.92 to 4.85, with the highest value (4.85) associated with Unit FL\_F (Table 2). The lowest ratio (2.92) relates to Unit FL\_E (Table 2). In general, higher  $SiO_2/Al_2O_3$  ratio characterises sedimentary stratigraphic units that are higher in sand particle size fractions than units that are muddy or composed more of fines or fine fractions. For instance, units FL\_A, FL\_B and FL\_E that are slightly ferruginous to ferruginous gravelly muddy sand have lower  $SiO_2/Al_2O_3$  ratios of 2.92–2.99 as compared with units FL\_C, FL\_D, FL\_F and FL\_G ( $SiO_2/Al_2O_3$  ratios vary from 4.06 to 4.85),

which are composed of thinly laminated sand to thickly laminated gravelly sand. The former units plot in the shale field near the boundary of the Fe-shale field in Herron's geochemical classification diagram, while the later units occur in the greywacke field (Figure 4).

The  $K_2O/Al_2O_3$  ratios for the analysed sediment samples vary from 0.127 to 0.215. The sedimentary units show a trend in the  $K_2O/Al_2O_3$  ratios that mimics the computed  $SiO_2/Al_2O_3$  ratios (Table 2).  $K_2O/Al_2O_3$  ratios (0.127–0.130) of units FL\_A, FL\_B and FL\_E are lower than the ratios (0.202–0.215) obtained for units FL\_C, FL\_D, FL\_F and FL\_G. The decrease in the computed ratios of  $SiO_2/Al_2O_3$  and  $K_2O/Al_2O_3$  from the sands (e.g. FL\_C, FL\_D, FL\_F, and FL\_G) to the mud-rich sediments (e.g. FL\_A, FL\_B and FL\_E) may not be attributed to the dilution effect of quartz. This contrasts with the results documented in a previous study for the beach sands from the western Gulf of Mexico, where quartz dilution results in a decrease in the ratios of  $SiO_2/Al_2O_3$  and  $K_2O/Al_2O_3$  from the very fine-grained Playa Azul sands to the coarser Nautla sands [28]. Overall, the observed decrease in the ratio of  $SiO_2/Al_2O_3$  for the studied sediments is in the order FL\_F > FL\_G > FL\_C > FL\_D > FL\_A > FL\_B > FL\_E. Consequently, the compositional maturity is in the order FL\_F > FL\_G > FL\_C > FL\_D > FL\_A > FL\_B > FL\_E. This deduction corroborates the results of the modal analysis, which shows the maximum and the lowest proportions of quartz grains (and matrix components) in FL\_F and FL\_E, respectively.

### Provenance

The analysed samples of stratigraphic fluvial units show  $Al_2O_3/TiO_2$  ratios that range from 16.5 to 38.8 (average: 26.6) (Table 2).  $Al_2O_3/TiO_2$  ratios, in earlier studies, have served as useful indicators of sediment precursors [28–30]. In addition, Ti is comparatively an immobile element and, as a result, is an important indicator of parent rock composition [5], and it occurs primarily in phyllosilicates [31]. The understanding that  $Al_2O_3/TiO_2$  ratios in shales are similar to those of the parent rocks is a major support for their use as source rock indicators, e.g. the study by Hayashi *et al.* [32]. Previous workers have suggested that sediments characterised by an  $Al_2O_3/TiO_2$  ratio <14 have

a mafic igneous protolith, and sediments associated with  $Al_2O_3/TiO_2$  ratios that vary from 19 to 28 are inferred to have a felsic igneous rock source [33]. Similarly, Hayashi *et al.* [32] have used high  $Al_2O_3/TiO_2$  ratios (>21) to suggest a felsic protolith source for the sedimentary rocks from northeastern Labrador, Canada. Accordingly, the units of the studied stratigraphic sequence have a predominantly felsic or felsic-to-intermediate igneous rock source. Similar results occur for the sandstones and shales from the Upper Kaimur Group in Central India, which show  $Al_2O_3/TiO_2$  ratios of 10.6–27 and which relate to felsic provenance [14].

Furthermore,  $K_2O$  and Rb have also been used to infer the provenance of clastic sediments (e.g. the works of Floyd and Leveridge [34] and Pe-Piper *et al.* [35]). Armstrong-Altrin *et al.* [28], in their study of the beach sands in the western Gulf of Mexico, used increases in the  $K_2O$  and Rb contents from Nautla (0.37, 10.5 ppm) to Tacolutla (1.22, 36.8 ppm) to Playa Azul (1.45, 37.9 ppm) sands to suggest a change in provenance from mafic to intermediate to felsic, respectively. In the current study, the sediment samples are comparatively enriched in  $K_2O$  and Rb contents, with values that range from 2.26 to 3.37 ppm and from 62.8 to 116 ppm, respectively. In concordance with the findings of Armstrong-Altrin *et al.* [28], the  $K_2O$  and Rb values in the analysed sediment samples suggest a felsic igneous rock source.

Previous studies show that REEs and Th occur in higher concentrations in felsic as compared with mafic igneous rocks. Conversely, Co, Sc and Cr concentrations are higher in mafic than in felsic igneous rocks. Therefore, the ratios of the elements serve as useful indicators of sediment source rocks (e.g. the works of Cullers *et al.* [36], Wronkiewicz and Condie [37], Condie and Wronkiewicz [38] and Cullers [39]). The usefulness of REEs, Sc and Th in inferring sedimentary rocks provenance is highly favoured by the minimal effect of fractionation of heavy minerals and processes of diagenesis and metamorphism, as compared with trace elements such as Zr, Hf and Sn [2, 37, 40]. In the current study, Sc and Lu have not been analysed in the sediment samples due to the analytical method adopted; hence, the study uses provenance discriminants that include the element

**Table 5:** Comparison of ratios of trace elements in the Geregu fluvial sediments with ratios in the sediments of felsic and mafic sources, as well as the upper continental crust

| Ratio of element | Geregu sediments <sup>a</sup> | Felsic sources <sup>b</sup> | Mafic sources <sup>b</sup> | Upper continental crust (UCC) <sup>c,d</sup> | Remarks                   |
|------------------|-------------------------------|-----------------------------|----------------------------|--|---------------------------|
| Eu/Eu*           | 0.64-0.92                     | 0.40-0.94                   | 0.71-0.95                  | 0.63 <sup>b</sup> , 0.72 <sup>c</sup>        | Dominantly felsic and UCC |
| La/Co            | 1.01-131.8                    | 1.80-13.8                   | 0.14-0.38                  | 1.76 <sup>b</sup>                            | Dominantly felsic and UCC |
| Th/Co            | 0.31-64.43                    | 0.67-19.4                   | 0.04-1.40                  | 0.63 <sup>b</sup>                            | Dominantly felsic and UCC |
| Th/Cr            | 0.069-0.383                   | 0.067-4.0                   | 0.002-0.045                | 0.13 <sup>b</sup>                            | Dominantly felsic and UCC |
| Cr/Th            | 2.61-14.42                    | 4.00-15.0                   | 25.0-500                   | 7.76 <sup>b</sup> , 8.76 <sup>c</sup>        | Dominantly felsic and UCC |

Note: <sup>a</sup>This study; <sup>b</sup>Cullers et al. [36], Mongelli [47], Cullers and Podkovyrov [9]; <sup>c</sup>McLennan [41] and Taylor and McLennan [16]; <sup>d</sup>Rudnick and Gao [42].

ratios La/Co, Th/Co, Cr/Th, Th/Cr and Eu/Eu\*. Results show that the ratios for La/Co, Th/Co, Cr/Th, Th/Cr and Eu/Eu\* obtained for the sediment samples favour felsic igneous rock source of upper continental crust composition than a mafic source (Table 5). Mishra and Sen [14] have stated that low Eu contents characterised felsic igneous rocks and, in this study, the analysed sediment samples have clear negative Eu anomaly (average Eu/Eu\* = 0.77), which suggests a felsic igneous rock source. According to Mishra and Sen [14], sediments characterised by Eu anomalies <0.85 are sourced from rocks of the upper continental crust. In addition, the negative Eu anomalies <0.85, coupled with (Gd/Yb)<sub>n</sub> ratios (1.53–1.82; average 1.65) <2.0, suggest a post-Archean protolith source for the analysed sediment samples [16, 43].

The plot of the trace element ratio La/Th versus Hf corroborates the aforementioned provenance discriminants (e.g. the work of Condie [31]). However, the sediment samples did not fall into the exact field but plot closer to the felsic source and upper continental crust field than the mixed felsic/basic source fields (Figure 9a). Additionally, sediment samples show high Hf content, which suggests that contributions of the old sediment part are greater in sediment sample FL\_A due to its high Hf content (20 ppm). Similarly, in the ternary plot of Th-Hf-Co, sediment samples did not plot in any of the provenance fields but plotted closer to the upper continental crust field than the oceanic crust field (Figure 9b). Consequently, the

analysed sediment samples are predominantly of a felsic igneous rock source that is of upper continental crust composition.

In the analysed sediment samples, FL\_B has the highest Cr concentration of 310 ppm, while the lowest concentration (30 ppm) occurs in the FL\_C unit. With respect to Ni, the highest (130 ppm) and lowest (10 ppm) concentrations occur in the FL\_B and FL\_F units, respectively. The comparatively high contents of Cr and Ni in Unit FL\_B as compared to other units of the sedimentary sequence may be associated with a greater adsorption onto clay minerals (e.g. the study by Young *et al.* [44]). The results of earlier studies for the Kudankulam sandstones [11] and floodplain sediments of the Kaveri River [45], southern India, document that Ni and Cr occur in concentrations as high as 50–130 ppm and 112–225 ppm, respectively, due to the effect of chemical weathering of mafic parent rocks (e.g. the studies by Armstrong-Altrin *et al.* [11], Singh and Rajamani [45]). In the analysed sediment samples, the observed content of Ni (10–130 ppm, average 60 ppm) and Cr (30–310 ppm, average 121 ppm) show mafic component contribution from the source area, even though this is not affirmed in the information obtained from other trace elements and REEs. Cr/Ni ratio is the lowest (0.5) for FL\_C and highest (7) in FL\_F. Cr/Ni ratios in units FL\_B (2.38), FL\_E (2.29), FL\_F (7) and FL\_G (2.5) are higher than in PAAS, which has a Cr/Ni value of 2.0. On the contrary, Cr/Ni ratios are lower in FL\_A (1.71), FL\_C (0.5) and FL\_D (1.5) as

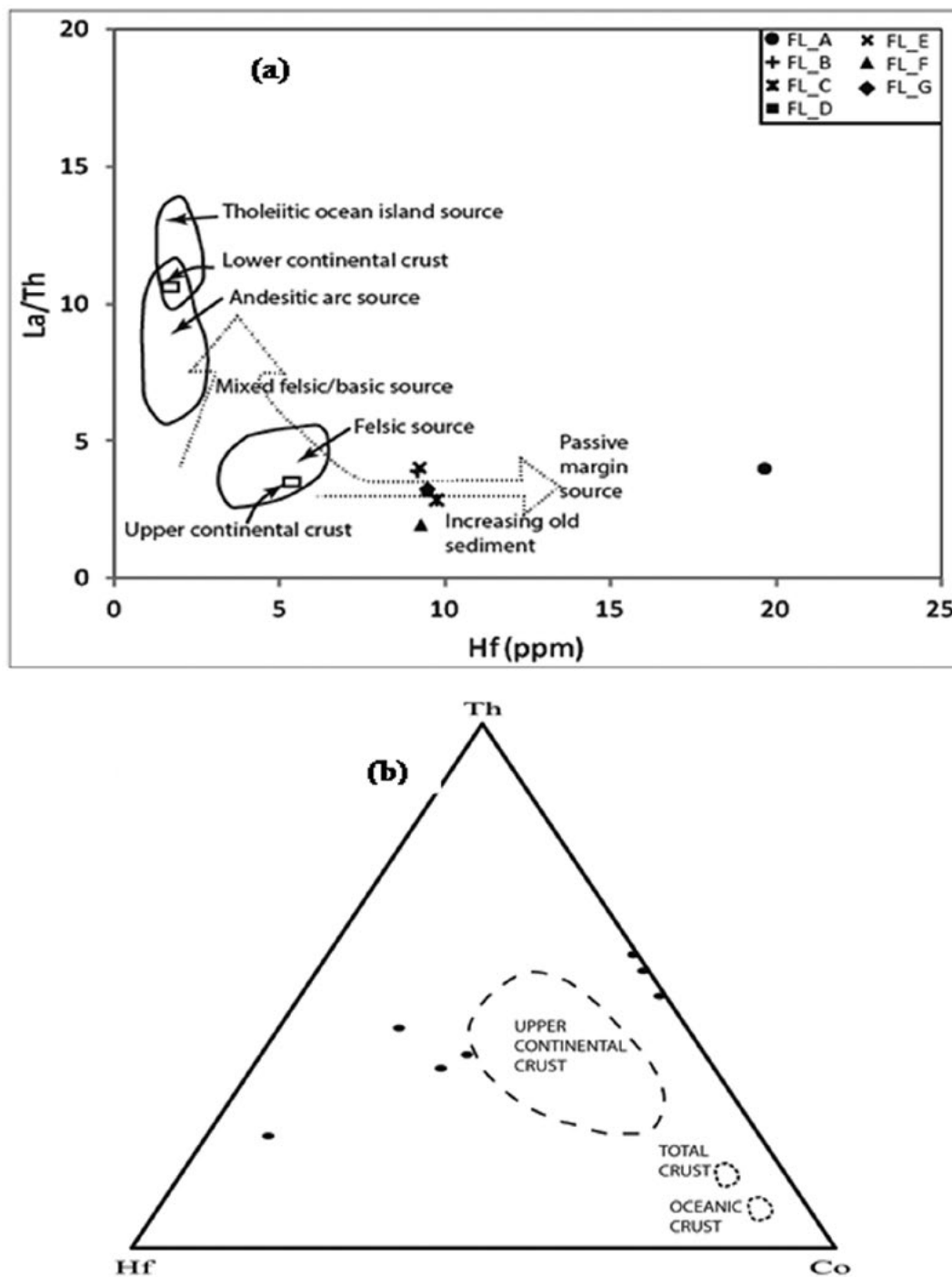


**Figure 9:** Trace element provenance discrimination diagrams for the fluvial sediments. (a) La/Th versus Hf discrimination plot (after Condie [31]). (b) Ternary Th-Hf-Co discrimination plot (after Taylor and McLennan [16]).

compared to PAAS. On average, the Cr/Ni ratio for the studied sediments is 2.55. The average Cr/Ni ratio obtained for the analysed sediment samples suggests lack of significant ultramafic-derived components from the source area (e.g. the works of Young *et al.* [44] and Garver

*et al.* [46]). In a previous study, it has been suggested that sediments have ultramafic igneous rock source when the Cr and Ni contents are >150 ppm and >100 ppm, respectively [46]. Elevated contents of Cr and Ni in sediments have also been used to infer an ultramafic source

**Table 6:** Tectonic setting discrimination for the Geregú fluvial sediments using REEs and element ratios (after Bhatia [1])

| Rare earth elements  | Geregú clastic sediments | Oceanic island arc | Continental island arc | Active continental margin | Passive margin |
|----------------------|--------------------------|--------------------|------------------------|---------------------------|----------------|
| $\Sigma$ REE         | 235                      | 58                 | 146                    | 186                       | 201            |
| Eu/Eu*               | 0.77                     | 0.93-1.15          | 0.66-0.92              | 0.6                       | 0.56           |
| (La/Yb) <sub>n</sub> | 9.53                     | 1.9-3.7            | 5-10                   | 8.5                       | 10.8           |

composition by previous workers [11, 28, 47, 48, 49]. According to Armstrong-Altrin *et al.* [28], the increase in Cr and Ni contents from Playa-Azul to Teculutla to Nautla sands, which corresponds to an increasing order in the Cr/Ni ratios, represents a more mafic source rock composition for the Nautla sand as compared with the other sands on the western Gulf of Mexico beach.

There is similarity in the REE patterns obtained for the analysed sediments, and this is a sign that they are probably sourced from the same parent rocks. The sediment samples have high LREE contents and have flat HREE patterns (Figure 8). Previous workers have used the REE pattern, coupled with the size of the Eu anomalies, to deduce whether sediments have felsic or mafic igneous rock sources [13, 16, 26, 37, 39, 50]. Previous workers have documented that mafic rocks are generally characterised by low LREE/HREE ratios and absence or insignificant negative Eu anomalies. On the contrary, felsic rocks exhibit high LREE/HREE ratios and discernible negative Eu anomalies [51]. It is, therefore, inferred that the fluvial sediments analysed in this study have a felsic protolith. This deduction corroborates the high LREE/HREE ratios (7.86–9.58) and sizeable Eu anomalies (0.64–0.92, average 0.77) that characterise the sediment samples.

### **Tectonic setting**

Previous studies have inferred sediments' tectonic settings by developing discrimination diagrams based on the major elements' (e.g. the works of Bhatia [1] and Roser and Korsch [3]) and trace elements' (e.g. the study by Bhatia and Crook [2]) geochemistry. The analytical package (UT-7 sodium peroxide fusion ICP-MS) used in this study did not analyse the Na, Sc and Zr contents in the sediment samples, which makes it impossible to apply the tectonic discrimination diagrams of previous reports

[2, 3, 52]. Nonetheless, the understanding from the work of Bhatia and Crook [2] shows that the analysed sediment samples are of a passive margin setting. The observable enriched LREE relative to HREE, coupled with the marked negative Eu anomaly (0.64–0.92, average 0.77), shown on the CI-chondrite-normalised plots of the analysed sediment samples closely resembles the characteristics of sediments deposited on passive margins, as documented by Bhatia and Crook [2]. Furthermore, the values of  $\Sigma$ REE, Eu/Eu\* and (La/Yb)<sub>n</sub> for the analysed sediment samples are closely analogous to those of passive margin depositional settings than those of oceanic island arc, continental island arc or active continental margin, which corroborates the aforementioned deduction (Table 6).

### **Conclusions**

The studied units of the stratigraphic sequence vary in maturity in the order FL\_F > FL\_G > FL\_C > FL\_D > FL\_A > FL\_B > FL\_E, and the variability is analogous to the pattern of decrease in ratios of SiO<sub>2</sub>/Al<sub>2</sub>O<sub>3</sub> and SiO<sub>2</sub>/K<sub>2</sub>O. A major control on the decrease in the computed ratios of SiO<sub>2</sub>/Al<sub>2</sub>O<sub>3</sub> and K<sub>2</sub>O/Al<sub>2</sub>O<sub>3</sub> from the sands (e.g. FL\_C, FL\_D, FL\_F and FL\_G) to the mud-rich sediments (e.g. FL\_A, FL\_B and FL\_E) is probably a consequence of the varying proportion of quartz grains and matrix components in the sediments.

The sedimentary units have a predominantly felsic igneous rock source of upper continental crust composition, with insignificant ultramafic inputs from the source area, corroborated by elemental ratios and REE composition. The protolith of the stratigraphic units is probably post-Archean as a result of the following observations: (Gd/Yb)<sub>n</sub> ratios <2.0, Eu anomalies <0.85 and similarity in REE patterns to those of PAAS. Marked negative Eu anomalies, cou-

pled with SREE and  $(La/Yb)_n$  composition of the sediments, suggest deposition in a passive margin tectonic setting.

## References

- [1] Bhatia, M.R. (1983): Plate tectonic and geochemical composition of sandstones. *Journal of Geology*, 91, pp. 611-627.
- [2] Bhatia, M.R., Crook, A.W. (1986): Trace element characteristics of greywacke and tectonic setting discrimination of sedimentary basins. *Contributions to Mineralogy and Petrology*, 92, pp. 181-193.
- [3] Roser, B.P., Korsch, R.J. (1986): Determination of tectonic setting of sandstone-mudstone suites using  $SiO_2$  content and  $K_2O/Na_2O$  ratio. *Journal of Geology*, 94, pp. 635-650.
- [4] McLennan, S.M. (1989): Rare earth elements in sedimentary rocks: Influence of provenance and sedimentary processes. *Reviews in Mineralogy*, 21, pp. 169-200.
- [5] McLennan, S.M., Hemming, S., McDaniel, D.K., Hanson, G.N. (1993): Geochemical approaches to sedimentation, provenance and tectonics. In: Johnson, M.J., Basu, A. (Eds.). Processes controlling the composition of clastic sediments. *Geological Society of America Special Paper* 284, pp. 21-40.
- [6] Condie, K.C. (1993): Chemical composition and evolution of upper continental crust: Contrasting results from surface samples and shales. *Chemical Geology*, 104, pp. 1-37.
- [7] Nesbitt, H.W., Young, G.M. (1996): Petrogenesis of sediments in the absence of chemical weathering: effects of abrasion and sorting on bulk composition and mineralogy. *Sedimentology*, 43, pp. 341-358.
- [8] Fedo, C.M., Young, G.M., Nesbitt, H.W., Hanchar, J.M. (1997): Potassic and sodic metasomatism in the Southern Province of the Canadian Shield: Evidence from the Paleoproterozoic Serpent Formation, Huronian Supergroup, Canada. *Precambrian Research*, 84, pp. 17-36.
- [9] Cullers, R.L., Podkovyrov, V.N. (2000): Geochemistry of the Mesoproterozoic Lukhanda shales in south-eastern Yakutia Russia: Implications for mineralogical and provenance control and recycling. *Precambrian Research*, 104, pp. 77-93.
- [10] Cullers, R.L., Podkovyrov, V.N. (2002): The source and origin of terrigenous sedimentary rocks in the Mesoproterozoic Ui Group, south-eastern Russia. *Precambrian Research*, 117, pp. 157-183.
- [11] Armstrong-Altrin, J.S., Lee, Y.I., Verma, S.P., Ramasamy, S. (2004): Geochemistry of sandstones from the Upper Miocene Kudankulam Formation, southern India: Implications for provenance, weathering, and tectonic setting. *Journal of Sedimentary Research*, 74, pp. 285-297.
- [12] Armstrong-Altrin, J.S., Verma, S.P. (2005): Critical evaluation of six tectonic setting discrimination diagrams using geochemical data of Neogene sediments from known tectonic setting. *Sedimentary Geology*, 177, pp. 115-129.
- [13] Etemad-Saeed, N., Hosseini-Barzi, M., Armstrong-Altrin, J.S. (2011): Petrography and geochemistry of clastic sedimentary rocks as evidence for provenance of the Lower Cambrian Lalun Formation, Posht-e-badam bloc, Central Iran. *Journal of African Earth Science*, 61, pp. 142-159.
- [14] Mishra, M., Sen, S. (2012): Provenance, tectonic setting and source-area weathering of Mesoproterozoic Kaimur Group, Vindhyan Supergroup, Central India. *Geologica Acta*, 10(3), pp. 283-293.
- [15] Anani, C., Moradeyo, M., Atta-Peters, D., Kutu, J., Asiedu, D. (2013): Geochemistry and provenance of sandstones from Anyaboni and surrounding areas in the voltaian basin, Ghana. *International Research Journal of Geology and Mining*, 3(6), pp. 206-212.
- [16] Taylor, S.R., McLennan, S.M. (1985): *The Continental Crust: Its Composition and Evolution*. Blackwell: Oxford.
- [17] Kogbe, C.A. (1976): *Geology of Nigeria*. Elizabethan Publishing Company: Lagos.
- [18] Adiotomre, E.E., Ejeh, O.I., Adaikoph, E.O. (2014): Temporal variation in the textural characteristics of clastic sediments from Geregu, Ajaokuta, Nigeria. *International Journal of Scientific and Engineering Research*, 5(8), pp. 60-65.
- [19] Ajibade, A.C., Woakes, M., Rahaman, M.A. (1987): *Proterozoic crustal development in Pan-African regime of Nigeria*. In: Proterozoic Lithospheric Evolution, Kröner, A. (ed.). American Geophysical Union: Washington; pp. 231-259.
- [20] Ajibade, A.C., Fitches, W.R. (1988): *The Nigerian Precambrian and the Pan African orogeny*. In: Precambrian Geology of Nigeria, Oluyide, P.O., Mbonu, W.C., Ogezi, A.E., Egbuniwe, I.G., Ajibade, A.C., Umeji, A.C. (eds.). Geological Survey of Nigeria: Kaduna; pp. 45-53.
- [21] Elueze, A.A. (2000): Compositional appraisal and petrotectonic significance of the Imelu banded ferruginous rock in the Ilesha schist belt, southwestern Nigeria. *Journal of Mining and Geology*, 36 (1), pp.8-18.



- [22] Gazzi, P. (1966): Le arenarie del flysch sopracretaceo dell'Appennino modense: Correlazioni con il flysch di Monghidoro. *Mineralogica et Petrographica Acta*, 12, pp. 69-97.
- [23] Dickinson, W.R. (1970): Interpreting detrital modes of graywacke and arkose. *Journal of Sedimentary Petrology*, 40(2), pp. 695-707.
- [24] Herron, M.M. (1988): Geochemical classification of terrigenous sands and shales from core or log data. *Journal of Sedimentary Petrology*, 58 (5), pp. 820-829.
- [25] Barat, J., Zanda, B., Moynier, F., Bollinger, C., Liorzou, C., Bayon, G. (2012): Geochemistry of CI-Chondrites: Major and trace elements, and Cu and Zn Isotopes. *Geochimica et Cosmochimica Acta*, 83, pp. 79-92.
- [26] Tang, Y. Sang, L., Yuan, Y., Zhang, Y., Yang, Y. (2012): Geochemistry of Late Triassic politic rocks in the NE part of Songpan-Ganzi Basin, western China: Implications for source weathering, provenance and tectonic setting. *Geoscience Frontiers*, 3(5), pp. 647-660.
- [27] Le Maitre, R.W. (1976): The chemical variability of some common igneous rocks. *Journal of Petrology*, 17, pp. 589-637.
- [28] Armstrong-Altrin, J.S., Lee, Y.I., Kasper-Zubillaga, J.J., Carranza-Edwards, A., Garcia, D., Eby, G.N., Balaram, V., Cruz-Ortiz, N.L. (2012): Geochemistry of beach sands along the western Gulf of Mexico, Mexico: Implication for provenance. *Chemie der Erde*, 72, pp. 345-362.
- [29] Garcia, D., Fonteilles, M., Moutte, J. (1994): Sedimentary fractionations between Al, Ti and Zr and the genesis of strongly peraluminous granites. *Journal of Geology*, 102, pp. 411-422.
- [30] Anderson, P.O.D., Worders, R.H., Hodgson, D.M. Flint, S. (2004): Provenance evolution and chronostratigraphy of a Palaeozoic submarine fan-complex: Tanqua Karoo Basin, South Africa. *Marine and Petroleum Geology*, 21, pp. 555-577.
- [31] Condie, K.C. (1992): *Proterozoic terrains and continental accretion in southwestern North America*. In: Proterozoic Crustal Evolution, Condie, K.C. (ed.). Elsevier Scientific Publishers: Amsterdam, pp. 447-480.
- [32] Hayashi, K., Fujisawa, H., Holland, H.D., Ohmoto, H. (1997): Geochemistry of 1.9 Ga sedimentary rocks from northeastern Labrador, Canada. *Geochimica et Cosmochimica Acta*, 61, pp. 4115-4137.
- [33] Girty, G.H., Ridge, D.L., Knaack, C., Johnson, D., Al-Riyami, R.K., (1996): Provenance and depositional setting of Palaeozoic chert and argillite, Sierra Nevada, California. *Journal of Sedimentary Research*, 66, pp. 107-118.
- [34] Floyd, P.A., Leveridge, B.E. (1987): Tectonic environments of the Devonian Gramscatho basin, south Cornwall: framework mode and geochemical evidence from turbidite sandstones. *Journal of Geological Society of London*, 144, pp. 531-542.
- [35] Pe-Piper, G., Triantafyllidis, S., Piper, D.J.E. (2008): Geochemical identification of clastic sediment provenance from known sources of similar geology: the Cretaceous Scotian Basin, Canada. *Journal of Sedimentary Research*, 78(9), pp. 595-607.
- [36] Cullers, R.L., Basu, A., Suttner, I.J. (1988): Geochemical signature of provenance in sand-size material in soils and stream sediments near the Tobacco Root batholiths, Montana, USA. *Chemical Geology*, 70, pp. 335-348.
- [37] Wronkiewicz, D.J., Condie, K.C. (1989): Geochemistry and provenance of sediments from the Pongola Supergroup, South Africa: Evidence for a 3.0-Ga-old continental craton. *Geochimica et Cosmochimica Acta*, 53, pp. 1537-1549.
- [38] Condie, K.C., Wronkiewicz, D.J. (1990): The Cr/Th ratio in Precambrian pelites from the Kaapvaal Craton as an index of craton evolution. *Earth and Planetary Science Letters*, 97, pp. 256-267.
- [39] Cullers, R.L. (1994): The controls on the major and trace element variation of shales, siltstones and sandstones of Pennsylvanian-Permian age from uplifted continental blocks in Colorado to platform sediment in Kansas, USA. *Geochimica et Cosmochimica Acta*, 58, pp. 4955-4972.
- [40] Cullers, R.L. Chaudhuri, S., Kilbane, N., Koch, R. (1979): Rare earths in size fractions and sedimentary rocks of Pennsylvanian-Permian age from the mid-continent of USA. *Geochimica et Cosmochimica Acta*, 43, pp. 1285-1302.
- [41] McLennan, S.M. (2001): Relationships between the trace element composition of sedimentary rocks and upper continental crust. *Geochemistry, Geophysics and Geosystems*, 2, Paper Number 2000GC000109.
- [42] Rudnick, R.L., Gao, S. (2003): *Composition of the continental crust*. In: The Crust, 3, L.R., Rudnick (ed.). Elsevier-Pergamon: Oxford; pp. 1-64.
- [43] Slack, J.F., Stevens, P.J. (1994): Clastic metasediments of the Early Proterozoic Broken Hill Group, New South Wales, Australia: Geochemistry, provenance and metallogenic significance. *Geochimica et Cosmochimica Acta*, 58, pp. 3633-3652.
- [44] Young, S.M., Pitawala, A., Ishiga, H. (2013): Geochemical characteristics of stream sediments, sediment fractions, soils, and basement rocks from the Ma-

- hawali River and its catchment, Sri Lanka. *Chemie der Erde-Geochemistry*, 73, pp. 357-371.
- [45] Singh P., Rajamani V. (2001): Geochemistry of the floodplain sediments of the Kaveri River, southern India. *Journal of Sedimentary Research*, 71, pp.50-60.
- [46] Garver J.L., Royce, P.R., Smick, T.A. (1996): Chromium and nickel in shale of the Taconic Foreland: A case study for the provenance of fine-grained sediments with an ultramafic source. *Journal of Sedimentary Research*, 66, pp. 100-106.
- [47] Mongelli, G. (2004): Rare-earth elements in Oligo-Miocene pelitic sediments from Lagonegro Basin, southern Apennines, Italy: implications for provenance and source area weathering. *International Journal of Earth Sciences*, 93, pp. 612-620.
- [48] Ghosh, S., Sarkar, S. (2010): Geochemistry of Permian-Triassic mudstone of the Satpura Gondwana basin, central India: clues for provenance. *Chemical Geology*, 277, pp. 78-100.
- [49] Perri, F., Critelli, S., Mongelli, G., Cullers, R.L. (2010): Sedimentary evolution of the Mesozoic continental redbeds using geochemical and mineralogical tools: the case of Upper Triassic to Lowermost Jurassic Monte di Gioiosa mudrocks (Sicily, southern Italy). *International Journal of Earth Sciences*, 100, pp. 1569-1587.
- [50] Cullers, R.L. (2000): The geochemistry of shales, siltstones and sandstones of Pennsylvanian-Permian age, Colorado, USA: Implications for provenance and metamorphic studies. *Lithos*, 51, pp. 181-203.
- [51] Cullers, R.L., Barrett, T., Carlson, R., Robinson, B. (1987): Rare earth element and mineralogical changes in Holocene soil and stream sediment: A case study in the Wet Mountains, Colorado, USA. *Chemical Geology*, 63, pp. 275-297.
- [52] Kroonenberg, S.B. (1994): Effects of provenance, sorting and weathering on the geochemistry of fluvial sands from different tectonic and climatic environments. In: Proceedings of the 29th International Geological Congress, Part A, pp. 69-81.